Triptolide self-assembling nanoparticles engineering with modified erythrocyte membranes for targeting and remodeling inflammatory microenvironment in arthritis

Jing Li[1], *Sanpeng Li*[1], *Chunbin Li*[1], *Hongfeng Li*[1], *Chuangjun Liu*[1], *Qi Zhao*[3], *Pengfei Zhang*[1*], *Ping Gong*[1,2*], *Lintao Cai*[1*]

1Guangdong Key Laboratory of Nanomedicine, CAS-HK Joint Lab for Biomaterials, Shenzhen Institutes of Advanced Technology, Chinese Academy of Sciences, Shenzhen 518055, China

2Guangdong Key Laboratory for Research and Development of Natural Drugs, Guangdong Medical University, Dongguan, 523808, China

3 Faculty of Health Sciences, University of Macau, Taipa, Macau, China.

[*]Corresponding author: Lintao Cai: E-mail: lt.cai@siat.ac.cn;

Ping Gong: E-mail: ping.gong@siat.ac.cn

Abstract

Overview: Rheumatoid arthritis (RA) is an autoimmune disease characterized by persistent synovitis, systemic inflammation and causing severe joint damage. Inflammation and influx of immune cells is a hallmark of the disease. Triptolide with great immunosuppressive activities is a potential drug to treat RA. However, its severe toxicity is still an unresolved bottleneck and largely limits its clinical use. Recently, nanoparticle (NP)-based drug delivery systems have been developed for detoxification of toxic drugs and diseases management.

Aim: To synthesize triptolide nanoparticles to decline its toxicity and improve water-solubility and develop a dual targeted biomimicking delivery system which targets to inflammation microenvironment. Finally, to achieve excellent therapeutic effect in rheumatoid arthritis.

Methods: We synthesized an amphiphilic molecule prodrug with the addition of diphenylalanine peptide (FF) to triptolide. These prodrugs were self-assembled into nanoparticles (TPNs) in water, then TPNs were coated with mannose-modified erythrocyte membranes to form a dual targeting manRTPNs. Specifically, mannose and natural molecule CD58 on RBC membrane guide it towards activated macrophages and T cells in inflamed joint through innate and specific immune recognition, respectively. Different cell lines including RAW264.7, CTLL-2, RSC364 and hFLS-RA and a collagen induced arthritis (CIA) mice model were used to detect the targeting and therapeutic effect in *vitro* and *vivo*.

Results: manRTPNs showed an excellent dual targeting ability to activated macrophages and T cells *in vitro*. We found that manRTPNs selectively induced anomalous activated cells death and indeed altered genes expression and cytokines production of inflamed cells such as macrophages, T cells and synoviocytes. In CIA mice, manRTPNs exhibited significantly targeting effect and prolonged drug accumulation at inflamed joints, whereby increased drug achieved significant therapeutic effect without adverse effect. In detail, manRTPNs ameliorated joint destruction, swollen paws considerably shrunk to normal, bone and cartilage destruction were suppressed and bone density was even recovered to healthy level. Basically, several core genes like *NF-κB*, *cox-2*, *rank*, *rankl*, *vegf*, *vegfr2*, *mmps*, and cytokines such as IL-6, TNF-α involved in inflammation, cartilage/bone destruction and angiogenesis were regulated and altered expression and production. Thus, the inflammation microenvironment was remodeled by TPNs.

Conclusion: This study demonstrated phenylalanine dipeptide mediating triptolide self-assembled nanoparticles to solve current problems and the potential of engineered RBC membranes for inflammation-targeted drug delivery. Therefore, our work is a good example of triptolide reconstruction, and this agent based on immune recognition may provide an immune cell targeted strategy for rheumatoid arthritis therapy.

Keywords: triptolide, nanodrug, dual targeting, inflammatory microenvironment, rheumatoid arthritis

Graphical Abstract

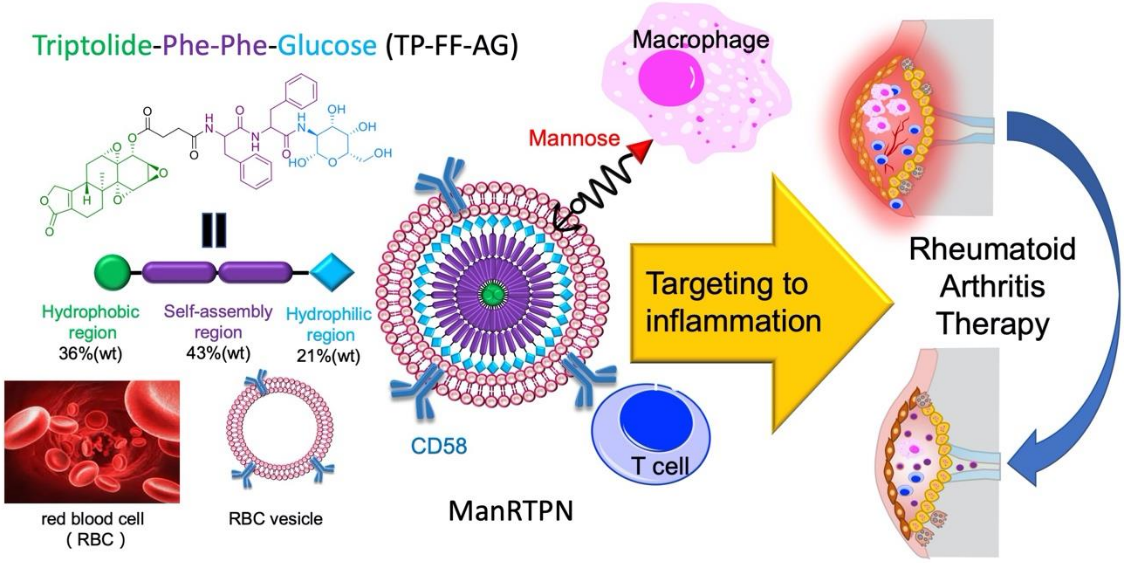

A novel triptolide nanodrug based therapeutic agent for RA management that modified erythrocyte membranes as a develiry system capable of dual targeted and triptolide remodeling inflammatory microenvironment in arthritis.

Introduction

Rheumatoid arthritis (RA) is a serious long-term disease characterized by persistent synovitis, systemic inflammation and autoantibodies and causing severe joint damage, disability and decreased quality of life. The etiopathogenesis remains elusive, and viable and effective treatment options are still limited[1]. Over the last two decades, long-term management of RA has involved disease-modifying anti-rheumatic drugs (DMARDs), biological agents such as tumor necrosis factor (TNF) inhibitors, and glucocorticoids[2]. Although the highest clinical remission rate achieved within 50% of control, not all patients attain desirable levels of clinical remission[3] and clinical use of these therapies is limited because of their high cost and frequency of adverse effects. The latter includes teratogenicity and hepatotoxicity of DMARDs like methotrexate[4, 5], risks of infections such as tuberculosis and osteoporosis caused by biological agents[6, 7] and long-term adverse reactions to glucocorticoid therapy[8, 9]. Lately, new therapies based on inflammatory cells such as macrophages and neutrophil or their products such as cell-free DNA in inflamed joint have been reported[10-12], however inhibiting a single factor may not be enough to sustainably halt or reverse disease progression due to RA's complexity and heterogeneity. Therefore, a new systemic design for drug candidate based on nano-medicine is urgently needed.

Triptolide is a trace natural triepoxide diterpene from *Tripterygium wilfordii* (or *Léi Gōng Téng*) and has been widely used to treat for RA patients since the 1970s in China[13]. Despite its various biological activities, low water solubility and severe toxicity, especially to the liver and kidney, remarkably impedes the translation to clinical applications[14]. Considerable efforts in structural modification[15-18] and nanoparticle(NP) -based drug delivery system [19-21] have been applied to reduce its toxicity. Unfortunately, common practices that direct conjugations attached to the C^{14}-hydroxyl group of triptolide via a hydrolytic ester bond have proven biologically unstable; meanwhile, current targeted drug-loading delivery systems are limited by drug loading or encapsulation ratio and they mostly target to kidney or tumor[22]. Therefore, an effective and stable system that can deliver triptolide to other organ or tissue such as joint is necessary. But until now, triptolide-formed nanoparticles have been rarely reported before. From this point, inspired from biomacromolecule self-assembly process, various peptide building blocks have been performed for the creation of biomimetic or bioinspired nanostructured materials[23, 24]. Recently, diphenylalanine (FF) is the simplest peptide building block for self-assembly and exhibits remarkable advantages including biocompatibility and non-immunogenicity and so on. Many researchers have developed FF-based nanomaterials such as nanotubes, spherical vesicles, nanofibrils and nanowires[25]. However, it is barely to link it with toxic drug for nanodrug formation. Therefore, diphenylalanine (Phe-Phe, FF) mediating self-assembling nanoparticles is a new strategy to reconstruct triptolide to be nanoparticles whose spherical nanostructure was more stable and biocompatible than before.

In RA pathogenesis, numerous blood-derived cells infiltrate in synovium and cytokine secret necessitates formation of new blood vessels to generate pannus, that all of these form an inflammatory microenvironment[26]. Peripheral-blood monocytes are recruited to joint, and functionally diverse macrophages distribute in the synovial sublining and lining layers. It is mentioned that Cluster of Differentiation 206 (CD206) on macrophages surface has been induced to express more [27]. Besides, prominent T cells being activated, especially the $CD4^+$ subset, also infiltrate the synovium. As reported, certain signal proteins on the T cell surface such as lymphocyte function antigen 2 (LFA-2/CD2) have increased in both RA patients and animal models[28, 29]. It was reported that CD2 can be effectively targeted by peptides derived from LFA-3/CD58 as well as fusion protein constructs. Interestingly, the ligand of CD2 namely CD58 widely distributes on erythrocyte membranes and CD58-CD2 interaction have mediated process of T cells activation[30]. These immunological characteristics of erythrocytes scarcely ever attracts attention in application, so it is a valuable attempt to apply in drug targeting. Then, mannose, the ligand of CD206 was introduced in erythrocyte membrane for ligand-binding targeting. In addition, the long circulation and flexible functionalization of erythrocyte membrane also make it be a promising platform and have wide application[31, 32]. In this study, we prepared mannose-labeled RBC membrane to entrap newly synthesized triptolide nanoparticles (TPNs) for elevating its vast retention in inflammation and achieving remarkably anti-inflammatory therapy. Triptolide, a hydrophobic drug, was linked with diphenylalanine peptide to self-assembly into size-controlled nanoparticles (TPNs) in water, and this reconstruction has successfully decreased its toxicity and improved water-solubility. As shown in scheme 1, the nanodrug core was coated with decorated RBC membranes to obtain mannose-modified RBC cell membrane-coated triptolide nanoparticles (manRTPNs). By translocating RBC membranes to the nanoparticles, the biological targeting properties of RBC cell can be conferred to manRTPNs as well, allowing them to target activated T cells through the CD58-

CD2 affinity. Further, the binding interaction between the mannose and its receptor CD206 enhanced anchoring of manRTPNs to activated macrophages. According to manRTPNs, the dual-targeting strategy facilitated the accumulation of nanodrug in inflammation, and the accumulated TPNs efficiently achieved systemic administration of rheumatoid arthritis by specifically inducing cell death and remodeling the inflammatory microenvironment through affecting genes network, downregulating cytokines and pro-angiogenic factors, regulating osteoclastogenesis, and returning balance of metalloproteinases and their inhibitors. Overall, our study expanded the RBC cell membrane biological application in nanocarrier for targeting inflammation through innate and specific immune recognition, and the triptolide nanodrug showed high drug content, low side effect, good biocompatibility which showed great potential for further inflammation diseases therapy.

Results and Discussion

Preparation and characterization of manRTPNs

Triptolide is a diterpene triepoxide with several active sites that can be modified, especially C_{14} position[33]. Because of its hydrophobicity, triptolide molecule acts as self-assembly inducer with the addition of diphenylalanine peptide (FF), which is the key moiety of the self-assembling peptide-drug conjugate. Initially, we added a glucosamine (AG) to the FF terminal to lengthen the hydrophilic chain, and then linked triptolide to FF-AG by an ester bond whose cleavage led to drug release in the cell; thus, the self-assembling monomer (TP-FF-AG) as a triptolide prodrug was synthesized (Figure 1A). The chemical structures of these compounds were confirmed via mass spectrometry (MS) and nuclear magnetic resonance

(NMR; Figure S1-S16). Due to hydrophobic interactions, triptolide nanoparticles (TPNs) were formed via self-assembly of synthesized monomer namely TP-FF-AG, which is uniformly easy to control TPNs size in water solution. The particles morphology was observed via transmission electron microscopy (TEM; Figure 1B). To synthesize manRTPNs, RBC membranes were extracted by hypotonic hemolysis[34], and mannose inserted by PEG_{2000}-DSPE. An extruder was using to camouflage mannose-modified erythrocyte membranes onto TPNs then form a core-shell structure (Figure 1B). Dynamic light scattering (DLS) measurements revealed that the TPNs were 135 nm in hydrodynamic diameter and manRTPNs were about 10 nm larger with PDIs of 0.15-0.2. The surface zeta potential of the shell was not as negative as that of the cores but was comparable to that of erythrocyte membrane-derived vesicles (RBC vesicles) (Figure 1C). All these results demonstrated successful cloaking of TPNs with erythrocyte membranes.

Next, TPNs and manRTPNs were stored in phosphate-buffered saline (PBS) for 1 month, where they demonstrated a negligible change in size and showed an excellent stability (Figure 1D). Maintaining protein compounds of erythrocyte membranes on nanoparticles' surfaces is vital for harnessing their biofunctionality. Therefore, completeness of the membrane coating was verified via sodium dodecyl sulfate polyacrylamide gel electrophoresis (SDS-PAGE; Figure S17), which indicated the manRTPNs maintained the whole effective biocomponent of erythrocyte on the surface. Translocation of erythrocyte membranes might improve the biocompatibility and circulating period of TPNs in vivo, which also sustains systemic delivery and better targeting through both passive and active uptakes[35]. As reported, the elimination

$T_{1/2}$ of triptolide molecules in rats following *i.v.* administration was 15-21 minutes, which showed that drugs were rapidly eliminated[36]. However, TPNs and manRTPNs have maintained higher plasma concentration after tail intravenous injection of mice in our work. As the relative signal of drug down to 50%, TPNs lasted 4 h, and manRTPNs even had a much longer elimination half-life of over 48 hrs (Figure 1E), which suggested that manRTPNs significantly expanded blood circle compared to triptolide. Therefore, the self-assembling TPNs nanostructure was more stable than original drug, and manRTPNs inherited biological properties of erythrocyte membrane proteins for following efficacy.

Dual-Targeting capacity and immunosuppressive effect of manRTPNs

To determine each targeting capacity of manRTPNs to macrophage and T cell *in vitro*, nanoparticles were Cy5.5-labelled and incubated with RAW264.7 and CTLL-2 treated with IL-4 (100 ng/mL) or TNF-α (10 ng/mL), untreated cells and RSC364 as control. Flow cytometry (FCM) analysis observed gradual increased uptake of nanoparticles by RAW264.7 and CTLL-2 for 6 hrs (Figure S18-20). An uptake curve was built using mean fluorescence intensity (MFI) of cells at six time points, and cellular uptake rate was defined as *k* indicated in figure 2A-C, which was the slope of the uptake curve. In detail, *k*s of nanoparticles in activated RAW264.7 and CTLL-2 were significantly higher than that in untreated cells (Figure 2A-C; Figure S21A & S22), and *k*s of manRTPNs were significantly higher than that to TPNs both in RAW264.7 and CTLL-2 (Figure 2A-B), but no difference of *k*s existed between TPNs and manRTPNs in RSC364 that no targeting ligands on it (Figure 2C). Further, the *k* value in RAW264.7 was higher than that in CTLL-2 (Figure 2A-B), indicating the affinity difference of interacted molecule pairs. To further confirm ligand-binding specificity, Cy5.5-labelled TPNs (without mannose and CD58), RTPNs (with CD58) and manRTPNs (with mannose and CD58) were incubated with treated macrophages and T cells for 3 hrs as well, RSC364 and hFLS-RA as control. After treatment, CLSM images showed that CD206 and CD2 (Figure 2D-E, green) respectively overexpressed on surface of RAW264.7 and CTLL-2. Significant red fluorescence was observed on RAW264.7 incubated with manRTPNs, but not with TPNs and RTPNs (Figure 2D), while red fluorescence was observed on CTLL-2 incubated with RTPNs and manRTPNs but not with TPNs (Figure 2E), which was consistent with corresponding ligands distribution on the nanoparticles. When co-incubated with RSC364, they also entered cells (Figure 2F; Figure S21b). Similar results were observed in flow cytometry analysis (Figure 2G-I; Figure S21c). These results demonstrated the ability of manRTPNs to target inflamed cells conferred by their mannose modified erythrocyte membrane coating, which is probably attributed to specific affinity of mannose-CD206 and CD58-CD2.

Except for migrated immune cells, synovial fibroblast is main resident effector of inflammation. To determine immunosuppressive efficacy of manRTPNs in joint inflammatory cells, LPS-treated RAW264.7, TNF-α-treated CTLL-2 and RSC364, and hFLS-RA were incubated with manRTPNs in 96-well plates for 24 hrs. Firstly, cell viability was measured via MTT assay. TPNs and manRTPNs didn't significantly reduce RAW264.7 viability even at a concentration of 500 nM (Figure 3A). However, at the same concentration CTLL-2, RSC364 and hFLS-RA showed an obvious cytotoxicity (Figure 3B-D). Specially, manRTPNs had an IC_{50} (half maximal inhibitory concentration) values of 219 nM for activated CTLL-2 cytoxicity, 88.9 nM for activated RSC364 cytoxicity and 95.8 nM for hFLS-RA cytoxicity (Figure 3B-D). The lower IC50 values of activated RSC364 and hFLS-RA indicated that triptolide-induced cell death was mainly against anomalous proliferative synoviocytes in inflamed joints, rather than lymphocytes like macrophages. Cells were following collected and lysed for mRNA extraction to check certain inflammation associated genes variation by qPCR. For LPS-treated RAW264.7, transcription factor *NF-κB* associated with most cytokine transcription[37] and *cyclooxygenase-2* (*cox-2*) were induced to decrease expression level, but *tissue inhibitor of metalloproteinase-1* (*timp-1*) showed opposite variation under manRTPNs treatment. *Receptor activator of NF-κB ligand* (*rankl*) over-expressed on TNF-α-treated CTLL-2 was also downregulated by manRTPNs. After activated with cytokines and chemokines, synovial fibroblasts release matrix-degrading enzymes, including matrix metalloproteinases (MMPs) and cathepsins causing cartilage and bone destruction[38]. In RSC364, the transcripts of metalloproteases such as MMP-2 and MMP-9 and vascular endothelial growth factor (VEGF) being critical for angiogenesis were lessen by manRTPNs as well (Figure 3E). Thirdly, medium supernatants were collected to measured cytokines by ELISA assay. supernatant IL-1β and IL-6 of LPS-treated RAW264.7 and supernatant IFN-γ of TNF-α-treated CTLL-2 lessened more quickly that treated with manRTPNs than TPNs (Figure 3F-H), while supernatant IL-1β and IL-6 of TNF-α-treated RSC364 had a similar decreasing curve between TPNs and manRTPNs groups (Figure 3I-J), which indicated that manRTPNs had superior identification of immune cells than resident synoviocytes at least in cytokine secretion. Consequently, manRTPNs selectively exerts its immunosuppressive effects on selectively inducing lymphocytes and synovial fibroblasts cell death, but also regulating production of proinflammatory cytokines, proinflammatory mediators and matrix metalloproteinases, which suggested manRTPNs may have an ability to remodel inflammatory microenvironment through its cell-specific anti-inflammation efficacy.

Targeting capacity and accumulation of manRTPNs *in vivo*

Upon the good capacity of manRTPNs to target activated macrophages and T cells in vitro, we further verified their ability to target RA site in vivo. After CIA mouse model being induced, all four paws swelled in varying degrees[39]. Hind paws were more heavily swollen, and micro-computed tomography (Micro-CT) imaging showed distinct bone loss of joint therein (Figure 4A). Then these mice received intravenous injections of free cyanine 5.5 (Cy5.5) solution and Cy5.5-labelled TPNs and manRTPNs for targeting imaging in vivo. As shown in figure 4A, almost no fluorescence signal was detected in paws of the free-Cy5.5 group, indicating that the dye barely accumulated at local inflammatory sites. In the TPNs group, we detected a weak signal, which peaked after 4 h (Figure 4A). While manRTPNs obviously reached the RA sites and lasted there for ≥12 hrs, which would be attributed to their long circulation and the targeting effect of the modified erythrocyte membranes. Thus, significant fluorescence of manRTPNs lasted longer and showed greater accumulation than that of TPNs. 24 hrs after intravenous injections, we dissected mouse and got froze sections of left paws to observe nanoparticles' retention in the inflamed joints. Contrary to free-Cy5.5 and TPNs group, fluorescence microscopy indicated a very high fluorescence intensity of manRTPNs in the synovial sublining layer, resulting in a reduced accumulation at the inflamed joint due to the lack of permeability

(Figure 4B). Tissue biodistribution further revealed manRTPNs' outstanding capacity to target the paws of RA mice, rather than other groups (Figure 4C). Additionally, higher accumulation was observed in liver, suggesting that this organ might be passive targeting of nanoparticles and the main organ metabolizing triptolide (Figure 4C). The results confirmed that the effective accumulation of manRTPNs provided a promising precondition of RA treatment.

Therapeutic efficacy of manRTPNs

The efficacy of ameliorating joint damage of manRTPNs was evaluated in a CIA mouse model. Following arthritis induction, CIA mice presented symptoms of swelling in ankle and paw joints and a clinical scoring was used to estimate the swelling degree (Figure S23). According to protocol timeline, CIA mice were treated with intravenous injections of triptolide at 15 mg/kg, TPNs and manRTPNs at doses of 25 mg/kg for 11 days (Figure 5A). Surprisingly, swollen hindpaws and forepaws both shrunk considerably and even recovered to the same extent as healthy ones with manRTPNs treatment rather than slightly shrunk in TPNs and triptolide group, but swelling symptoms of other groups were increasingly severe (Figure 5B), implying that inflammation process was exactly controlled by manRTPNs. As paw swelling is only a surface phenomenon of RA, bone loss was further determined using Micro-CT analysis. Reconstructed three dimensional (3D) bones images and calculated bone mean density (BMD) showed that serious bone erosion was suppressed and bone density even recovered to healthy mice level of manRTPNs treatment (Figure 5C-D), suggesting a protective role of manRTPNs on cartilage and bone damage. Haemotoxylin and eosin (H&E)-stained sections showed an intense anomalous proliferative cells infiltration in the joints and synovium of control groups.

By contrast, remarkable reduction of immune infiltration and preservation of cartilage were observed in manRTPNs group (Figure 5E). Further, cytokines including TNF-α and IL-6 are known to increase with the onset of arthritis and correlate strongly with disease severity[40]. Immunohistochemical analysis showed that TNF-α and IL-6 in synovium and articular cavity significantly declined in manRTPNs groups (Figure 7A-B) and serum levels of them also observed to alleviate similarly (Figure 6C), indicating effective reduction of arthritis at cytokines level. Moreover, gene heatmap showed that manRTPNs suppressed several genes expression including *rank*, *rankl*, *vegf*, *vegfr2*, *NF-κB*, *cox-2*, *IL-1β*, *mmp-2*, *mmp-3*, *mmp-9* and *mmp-13,* that these transcripts are dramatically increased and contribute in joints damage. Some negative regulators such as opg, timp1 and timp2 were upregulated their gene expression by manRTPNs (Figure 6D), indicating manRTPNs preserve appropriate and balanced concentration of cytokines and inflammatory factors through two-way regulation. RANKL/RANK/ORG signal pathway is key of bone metabolism[41]. The up-/down-regulation of manRTPNs also recovered the balance of RANKL/RANK/ORG and metalloproteinases and their inhibitors (TIMP) to normal. Thus, manRTPNs ameliorated destroyed through aiming to RA pathological factors including cytokines, extracellular matrix (ECM), bone metabolism and angiogenesis.

Biosafety of manRTPNs nanoparticles

To investigate safety and biocompatibility of TPNs and manRTPNs in vivo, we administered PBS, TPNs or manRTPNs at a single dose of 25 mg/kg to healthy mice via tail vein, while to other mice we administered triptolide (original drug of TPNs and manRTPNs) at

15 mg/kg by intraperitoneal injection. It is worth mentioning that most mice in the triptolide group died soon (within 24 hrs) after 25 mg/kg administration, indicating the high toxicity of the original drug (Figure S24). After 1-week treatment, mice treated with triptolide showed a significant decrease in count of white blood cells (WBC), RBCs and platelets (Figure 7A), suggesting the occurrence of bone marrow suppression, which is one of the main side effects of triptolide. The main three type cells comprised WBC including neutrophils, lymphocytes, and monocytes showed significant count differences between triptolide group and other groups, which explained the WBC count variation conferred from triptolide (Figure 7B). The hemoglobin concentration did not differ significantly among all the groups in the blood (HGB), mean corpuscular hemoglobin (MCHC) level, and hemoglobin distribution width (HDW) (Figure 7C), indicating that triptolide didn’t influence the physiological function of RBCs. Blood biochemistry analysis showed that blood urea nitrogen (BUN), aspartate aminotransferase (AST), creatinine (Cr) and lactate dehydrogenase (LDH) levels of mice treated with triptolide were significantly higher than those of mice in the TPNs and manRTPNs groups (Figure 7D-G). These variations demonstrated that the hepatotoxicity and nephrotoxicity of triptolide were greatly reduced in TPNs, with RBC membrane coating yielding even better safety. Hematoxylin and eosin (H&E) staining of major organs showed that triptolide treatment caused inflammatory infiltration of the liver and severe renal injury characterized by loss of the brush border, tubular epithelial cells detachment from the basement membrane and tubular obstruction. Meanwhile, the TPNs and manRTPNs groups showed no

significant variation in cellular morphology and negligible organ damage, in line with the PBS group (Figure 7H). However, TPNs and manRTPNs significant reduced triptolide toxicity.

Conclusion

Our study expanded the RBC cell membrane biological application in nanocarrier for targeting inflammation through innate and specific immune recognition, and the triptolide nanodrug showed high drug content, low side effect, good biocompatibility which showed great potential for further inflammation diseases therapy. Generally, there are two improvement of manRTPNs in cell-membrane-coated nanoparticle delivery system, namely triptolide nanodrug core and RBC membrane shell. RBC membrane-camouflaging nanoparticles has been extensive established platform, but there are still many deposits from RBC cell itself to further develop disease-targeting and therapy platform except for tumor. The natural immunological function of RBC cells has been always neglected in targeted drug delivery construction. So, taking advantage of adhesion molecules affinity between RBC cells and immunocytes in building nanocarrier for transporting drug to inflammation deeply expands application of established RBC membrane platform. On the other side, triptolide has excellent anti-inflammation and immunosuppressive effect and solving its low water-solubility and toxicity is premise of using it in various diseases management. Our reconstruction of triptolide isn't content-limited loading in micelles, but drug-based self-assembled size-controlled nanoparticles. This strategy takes advantages of drugs' hydrophobicity to solve its bad water-solubility, which is magic of nanotechnology. While inflammation is prevalent related with many diseases like cardiovascular diseases, gastrointestinal tract, cancer and pathogen infection[42]. Therefore, manRTPNs as a drug delivery system of inflammation targeting and treating may be a promising agent in other inflammation-associated diseases therapy.

Materials and methods

Animal care

Mice were housed in an animal facility at Shenzhen Institutes of Advanced Technology, Chinese Academy of Sciences (SIAT). All animal experiments were performed in accordance with Guidance Suggestions for the Care and Use of Laboratory Animals and approved by Sciences Animal Care and Use Committee of SIAT.

Erythrocyte membranes derivation

Erythrocyte membranes were collected according to a previously reported method with modification. Briefly, fresh heparinized whole blood was collected from male mice (20-22 g) and subsequently centrifuged at 2000 rpm for 15 min at 4 °C to remove the plasma and the white buffy coat. The collected red blood cells (RBCs) were washed with 1× PBS three times and suspended in 0.25× PBS for 2 hours at 4 °C, and then the hemoglobin was removed by centrifugation at 9,000 rpm for 45 min. The resulting pink pellet was purified with 1× PBS, and the collected erythrocyte membrane was suspended and stored in distilled water. To form ligand-inserted erythrocyte ghosts, the light pink solution was incubated with DSPE-PEG-mannose for 30 min, 37°C water bath. Erythrocyte membranes with PEG-mannose or not was further prepared by extruding through a 200 nm polycarbonate porous membrane with an Avanti mini-extruder (Avanti Polar Lipids).

Synthesis of TPNs

The TPNs were synthesized by a prodrug self-assembly method. Briefly, after dissolving 5mmol Boc-Phe-Phe-OH (BOC-FF, J&K scientific Ltd., China), 6 mmol 1-Ethyl-3-(3-dimethylaminopropyl) carbodiimide (EDC, J&K scientific Ltd., China) and 6 mmol N-Hydroxysuccinimide (NHS, J&K scientific Ltd.,China) in 3 mL anhydrous DMF, another anhydrous DMF solution containing 5.5 mmol glucosamine (AG, Sigma-Aldrich, USA) and 5 mmol TEA (J&K scientific Ltd., China) was added drop-wise into it. The mixture was evaporated under reduced pressure for 24 hours to get crude product BOC-FF-AG. Then, crude BOC-FF-AG was dissolved in 30 mL equal volume mixture of anhydrous dichloromethane and trifluoroacetic acid (TFA, J&K scientific Ltd., China) and stirred for 4 hours at room temperature. Afterward, pure NH_2-FF-AG was obtained after evaporated under reduced pressure and purified by silica gel column chromatography with dichloromethane and methanol. Secondly, 1 mmol triptolide (TP, Shanghai Yuanye Bio-Technology Co., Ltd., China), 1.2 mmol succinic anhydride (SAA, Sigma-Aldrich, USA) and 0.2 mmol dimethyl aminopyridine (DMAP, Sigma-Aldrich, USA) were dissolved in 3 mL pyridine and stirred overnight. After then, the mixture was diluted with ethyl acetate and washed it with solution containing saturated copper sulfate (J&K scientific Ltd.), water and brine. After reaction, residue TP-COOH was obtained through drying with anhydrous Na_2SO_4 and concentration with rotary evaporator. In the third step, TP-COOH, dicyclohexylcarbodiimide (DCC, Sigma-Aldrich, USA) and 1-hydroxy-5-pyrrolidinedione (NHS, J&K scientific Ltd., China) of equal molar ratio were dissolved into 3 mL anhydrous dichloromethane and stirred at room temperature for overnight. The final product TP-FF-AG was gained by reaction of activated TP-COOH and NH_2-FF-AG for overnight at room temperature and purified by analytical RP-HPLC and semi-preparative RP-HPLC with simultaneous detection at 265 nm. Analytical RP-HPLC was performed at room temperature on the Shimadzu LC 20 with UV detector SPD-20A using Inertsil ODS-SP column (4.6 x 250 mm, 5 µm, 100Å). The RP-HPLC gradient was started at 10% of B (CH_3CN, J&K scientific Ltd., China), then increased to 100% of B over 30 min (A: 0.1% TFA in water). Semi-preparative RP-HPLC was performed on the ULTIMAT 3000 Instrument (DIONEX). For fluorescence imaging experiments, cyanine5.5 (Cy5.5, Lumiprobe, USA) was linked to intermediate product of NH_2-FF-AG after esterification reaction to obtain Cy5.5-FF-AG in the same way. Ultimately, nanoparticles were self-assembled by added TP/Cy5.5-FF-AG dissolved in DMSO dropwise into PBS while vigorous stirring and dialysis for 2 days. ^{1}H NMR and ^{13}C NMR spectra were recorded with a Bruker VANCE III400 spectrometer (400 MHz). The high-resolution mass spectra (HR-MS) were measured on a Bruker Micro TOF II 10257 instrument. For membrane coating, nanoparticles were mixed with prepared membranes in ratio of 1:1. The resultant mixture was subsequently extruded nine times through a 200 nm polycarbonate porous membrane using an Avanti mini-extruder to yield the erythrocyte membranes-coating TPNs or mannose inserted erythrocyte membrane-coating TPNs (namely RTPNs or manRTPNs).

Nanoparticles Characterization

The hydrodynamic diameter and zeta potential of NPs suspended in 1 × PBS were measured by dynamic light scattering (DLS) (Zeta Plus, Brookhaven Instruments, USA). The morphologies of TPNs and manRTPNs were observed by transmission electron microscope (TEM, FEI spirit T12) at an accelerating voltage of 120 keV. The stability experiment of TPNs and manRTPNs in PBS was monitored by DLS over five weeks and stored at 4°C. The proteins retained on manRTPNs compared with those on the natural erythrocyte membrane were observed by SDS-PAGE. Briefly, 2 mg of erythrocyte membrane vesicles and manRTPNs were collected by centrifugation at 15,000g for 30 min, mixed in SDS sample buffer (Invitrogen, USA), and heated at 90 °C for 5 min. Then, 20 μL of each sample was run on a 10% SDS-polyacrylamide gel (Bio-Rad, SDS-PAGE Gel Preparation Kit, USA) at 120 V for 1 h, followed by Coomassie blue staining and imaging.

Pharmacokinetics

To evaluate the circulation half-life of TPNs and manRTPNs in vivo, 150 μL Cy5.5-labeled nanoparticles were injected into the tail vein of the mice (n = 3). Twenty microliters of blood were collected at 1, 5, 15, 30 min, and 1, 2, 4, 8, 24, 48, and 72 h following the injection. Each particle group contained 3-4 mice. The collected blood samples were diluted with 30 μL PBS in a 96-well plate before fluorescence measurement. Pharmacokinetics parameters were calculated to fit a two-compartment model and a one-way nonlinear model.

Drug toxicity analysis in vivo

Purchased from Vital River Laboratory Animal Technology Co. Ltd (Beijing, China), males BALB/c mice (6~8 weeks old) were randomly divided into four groups and intravenously injected with PBS, TPNs and manRTPNs at a single dosage of 25 mg/kg and triptolide of 15 mg/kg 4 times for eight days. A total of 7 days after last administration, all mice were euthanized, and blood was collected for and blood routine examination and biochemical parameters measurement, while main organs including heart, liver, spleen, lung, and kidney were excised and stained by H&E for histological analysis.

Cell culture

RAW264.7 cells, CTLL-2, RSC364 and hFLS-RA were purchased from the American Type Culture Collection (ATCC, USA) and cultured in Dulbecco's minimum essential medium (DMEM, Corning, USA) supplemented with 10% fetal bovine serum (FBS, Gibco, USA), 1% penicillin (100 IU/mL, Corning, USA), and streptomycin (100 μg/mL, Corning, USA) and placed at 37 °C in a 5% CO_2 humidified atmosphere. Cell lines were purchased with certification of authentication and free from Mycoplasma.

Quantification of cell targeting in vitro

A 6-well culture plate was prepared and RAW264.7, CTLL-2, RSC364 and hFLS-RA cells were implanted at a density of 5×10^5 cells/well. 12-16 hrs later, 80% of cell coverage was confirmed. 50 μL Cy5.5-labelled TPNs or manRTPNs was adding into prepared cells every hour for six hours, incubated with covering foil paper and collected them in the sixth hour. After digestion with trypsin (Gibco, USA), cells were put together and washed three times with ice-cold PBS, then underwent flow cytometry by FACS Canto II (BD Biosciences). The data was analyzed using FlowJo software. Mean fluorescence intensity (MFI) reflected amount of intake nanoparticles amount. An uptake curve was constructed with MFI and time, and a k value being the slope of uptake curve was defined as uptake rate to measure targeting capacity of nanoparticles.

Immunofluorescence assay of macrophages and T cells with nanoparticles

Cells were cultured with medium added recombinant mouse IL-4 (100 ng/mL, R&D System, USA) or recombinant TNF-α (10 ng/mL, R&D System, USA) for six hours and incubated with TPNs, RTPNs or manRTPNs for 3 hours. Afterward, cells were fixed with 4% paraformaldehyde (Sigma-Aldrich, USA) for 10 minutes, permeabilized with 0.1% Triton™ X-100 (Sigma-Aldrich, USA) for 10 minutes, blocked with 1% BSA for 1 hour and labeled with 2 μg/mL anti-mannose receptor/AF488 conjugated antibody (ab195191, Abcam) and rabbit anti-CD2/AF488 conjugated antibody (bs-2899R, Bioss) for 3 hours at room temperature. Nuclei were stained with DAPI. All manipulation must be away from light. The images were captured under confocal microscopy (Leica, TCS SP5).

Cellular cytotoxicity study

The cellular toxicities of TPNs and manRTPNs on macrophages, T cells, FLSs and hFLSs were determined by MTT assay using CCK-8 Kit. Cells were implanted in a 96-well culture plate at a density of 8 × 103 cells/well (5 replicates each treated group). After 12 hrs, PBS, TPNs and manRTPNs with concentrations of 10 nM, 50 nM, 100 nM, 200 nM, 500 nM were added into medium for further 24 hrs co-culture. Then the cells were mildly washed by PBS before added CCK-8 mixed solution. Then, the optical density in 450 nm was measured by Multiskan GO (Thermo Fisher Scientific).

Cytokines concentration analysis

The TNF-α, IL-6 and IFN-γ concentrations of cells culture supernatants were determined with ELISA Kit using mouse ELISA Kits (Biolegend, USA) as manipulation. Also, the TNF-α and IL-6 concentrations of mouse serum samples were determined with TNF-α and IL-6 ELISA Kits (Biolegend, USA). Briefly, Serum samples of treated mice were collected at the end of experiment and concentrations of TNF-α and IL-6 were quantified with ELISA kits. Specifically, the whole blood of mice was collected by submandibular bleeding into microtubes and allowed to clot at room temperature for 30 min. Samples were then centrifuged at 2,000g for 6 min to collect supernatant serum. Serum samples were immediately frozen at -20 °C until analysis by using mouse TNF-α and mouse IL-6 ELISA kits (Biolegend) within 3 days of collection.

Genes expression profiles analysis of cells

After treated with nanoparticles of serious concentrations, cells were harvested to isolate RNA. RNA was extracted with TRIzol reagent (Invitrogen, USA) according to the manufacturer's instructions. Complementary DNAs (cDNAs) were synthesized with QuantiTect Reverse Transcription Kit (QIAGEN K.K., Tokyo, Japan) and the specific gene transcripts were quantified by quantitative real-time PCR using QuantiTect SYBR Green PCR Kit (QIAGEN K.K., Tokyo, Japan) and analyzed with ABI 7500 real-time PCR system (Applied Biosystems, USA). The gene expression patterns along with concentration were highlight with heatmap by using TBtools package.

Collagen induced arthritis (CIA) mice model induction

Seventy-two female DBA/1 mice (6~8 weeks old) were purchased from Vital River Laboratory Animal Technology Co. Ltd (Beijing, China). All mice were maintained in a SF system which is room equipped with an air-filtering system, and the cages and water were sterilized. CIA was induced as previously reported study[39]. Briefly, bovine type II collagen (Chondrex, Redmond, WA, USA) was dissolved in 0.1M acetic acid overnight at 4°C. This was emulsified in an equal volume of complete Freund's adjuvant (Chondrex, Redmond, WA, USA). The mice were immunized intradermal at the base of the tail with 100 μL of emulsion containing 100 μg of type II collagen. On day 21, mice were boosted intraperitoneal with 100 μg type II collagen dissolved in phosphate buffered saline (PBS). Clinical scores of each hindpaws and forepaws of mice were obtained following the standard evaluation process[39]. In detail, no evidence of erythema and swelling occurred is score 0, erythema and mild swelling appeared is score 1, erythema and mild swelling extended from the ankle to the tarsals is score 2, erythema and moderate swelling extended from the ankle to metatarsal joints is score 3 and erythema and severe swelling encompassed the ankle, paws, and digits or ankyloses of the limb is score 4. Then total clinical scores of hindpaws and forepaws were calculated. At least six mice each group.

Nanoparticles targeting to inflamed joints

After CIA model was established, free Cy5.5, Cy5.5-labelled TPNs and manRTPNs were intravenously injected into the CIA mice (20 mg/kg, n = 4). Fluorescence images were obtained after 1, 2, 4, 8, 12, and 24 hours using an in vivo imaging system (IVIS, Caliper, USA). Then, the mice were sacrificed for ex vivo tissue/organs distribution analysis at the end of experiment. Meanwhile, the synovial tissue was dissected and dehydrated in 30% sucrose solution overnight and then cry-sectioned at 8 μm. The sections were stained with DAPI and washed twice.

Fluorescence images were obtained using a confocal microscope (Leica, TCS SP5). The fluorescence intensity of sections in different groups was calculated using software Image J.

manRTPNs treatment assay

According to CIA mice model conduction, starting at day 21, the clinical scores were calculated to make sure that CIA mice were almost equably and randomly divided into four groups, while healthy DBA/1 mice were set as control (n = 5). Five different agents namely PBS, RBC vesicle, triptolide, TPNs and manRTPNs were intravenously injected every two days. The timeline of whole therapy experiment from model making to the end was according to schematic diagram shown in figure 5A. The arthritis index of each group was recorded over time to evaluate treatment efficacy. At the end, the mice were sacrificed for further analysis.

Micro-CT imaging of mice paws

The knee and ankle joints of each experimental mouse hindpaws were scanned using micro-CT system (Bruker's SkyScan 1278, UK) to observe joint bone situation. Images were acquired at 55 kV, 72 μA and 300 ms/frame, with 360 views. The 3D structures of knee joint and ankle joint were reconstructed from 360 views and BDM was evaluated by corresponding SkyScan NRecon package. Analysis typically took around 15 min per joint for an experienced operator.

Histological analysis and immunohistochemical staining assay

At study endpoints, mice were euthanized and hind knee joints were collected for H&E staining and immunohistochemical staining. Briefly, the ankle and knee joints of scarified animals as well as their heart, liver, spleen, lung and kidney were fixed in 10% buffered formalin and then joints were incubated in decalcifying solution (4% hydrochloric acid in 4% formaldehyde) at room temperature for 7 days for decalcification. After paraffinization, microtome (Leica) slices of 8 μm were prepared and stained with haematoxylin and eosin, images were taken by using inverted microscope (Olympus, IX71, Japan) and the inflammatory cell infiltration in synovial tissues, bone and cartilage was evaluated by Image J software. After deparaffinization the slices were subjected to antigen recovery in 0.01 M sodium citrate buffer at 125 °C for 30 s, followed by 10 s at 90 °C, and then subjected to the endogenous peroxidase inactivation by covering tissue with 3% hydrogen peroxide for 5 min. After blocking non-specific binding sites with 10% goat serum in PBS, the slices were incubated with TNF-α/IL-6 monoclonal antibody (Invitrogen) with a dilution rate of 1:100, respectively, at 4 °C for 24 h. Then the slices were incubated with horseradish peroxidase (HRP)-conjugated secondary antibody with a dilution rate of 1:800 at 37 °C for 1 hour. Sections were developed using the DAB substrate and then counterstained with haematoxylin. The images were captured and analyzed by inverted microscope (Olympus, IX71, Japan) and Image J software.

Gene expression profiles analysis of tissues

The paws and ankles were dissected from mice on day 22 of arthritis, snap-frozen in liquid nitrogen, ground into powder, and homogenized. All procedure must be under RNase-free conditions. The RNA isolation and real-time PCR assay were carried out following the protocol following. Briefly, total RNA was extracted with TRIzol reagent (Invitrogen, Carlsbad, CA, USA) from the tissue homogenates according to the manufacturer's instructions. The total RNA (1 μg) was reverse transcribed to cDNA using the QuantiTect Reverse Transcription Kit

(QIAGEN, Japan) and the specific gene transcripts were quantified by quantitative real-time PCR using QuantiTect SYBR Green PCR Kit (QIAGEN K.K., Tokyo, Japan) and analyzed with ABI 7500 real-time PCR system (Applied Biosystems, USA). PCR was performed as 40 cycles at 94°C for 15 s, 55°C for 30 s, and 72°C for 30 s. The relative RNA expression was calculated with comparative CT method; β-actin as internal ontrol. The gene expression patterns along with concentration were highlight with heatmap by using TBtools package. Gene-specific primers were synthesized by Sangon Biotech (Shanghai) Co., Ltd. and list in the TableS1.

Statistical Analysis

All the results are reported as mean ± SD. The differences among groups were analyzed using one-way ANOVA analysis and Student's t-test; *represents $P < 0.05$, ** represents $P < 0.01$.

Acknowledgments

This work was supported by National Natural Science Foundation of China (81801838, 31571013, 81701816 and 81601552), Guangdong Natural Science Foundation of Research Team (2016A030312006), K.C. Wong Education Foundation (GJTD-2018-14), Natural Science Foundation of Guangdong Province (2018A030313013), Shenzhen Science and Technology Program (JCYJ20180302145912832, JCYJ20160429191503002, JCYJ20170818162259843 and JCYJ20170818163739458). We thank Pro. Hongchang Li and Dr. Yifan Ma of SIAT for their useful and meaningful recommendations to improve this paper, and thank Mr. Danhui Quan for his help in some drawing.

Competing Interests

The authors have declared that no competing interest exists.

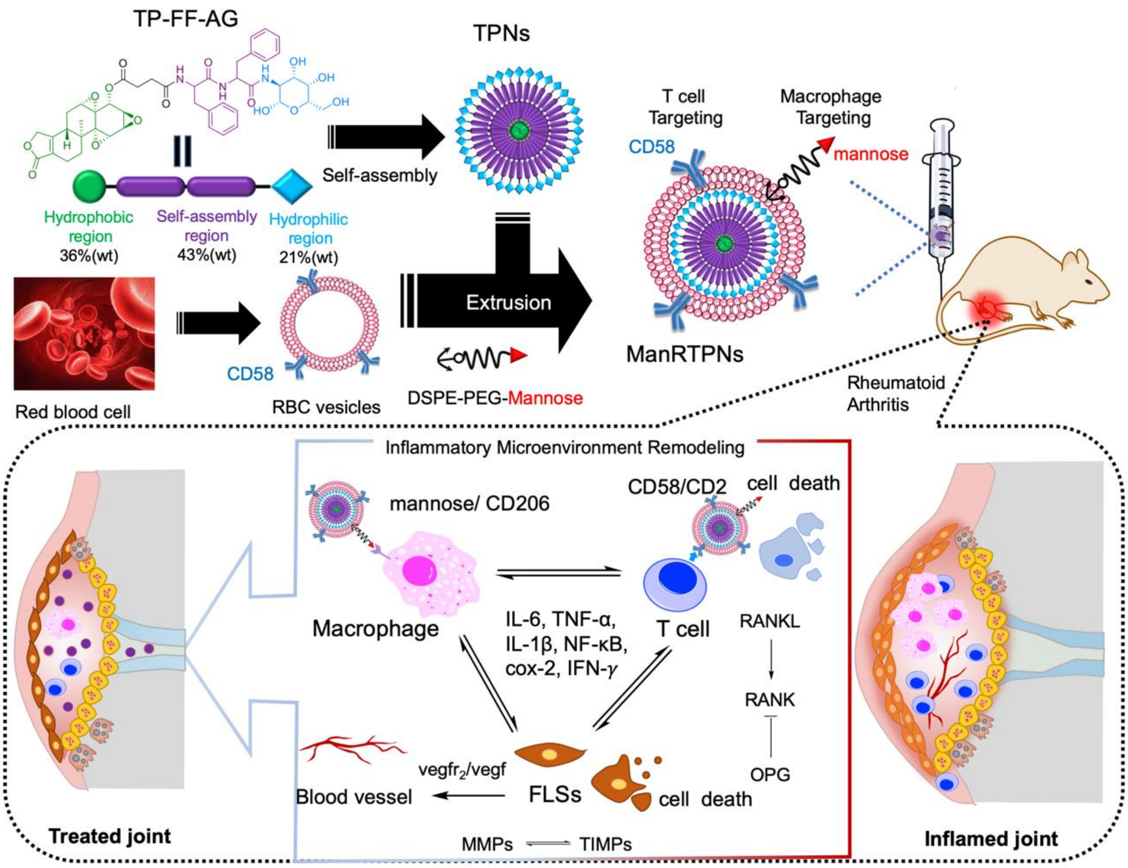

Scheme 1. Schematic illustration of mannose modified erythrocyte membranes-coated triptolide nanoparticle (manRTPNs) targeting to inflammatory sites of rheumatoid arthritis and significant therapeutic effect. Targeting capacity to macrophages and T cells of manRTPNs is conferred from the mannose modified erythrocyte membrane. Specifically, target activated T cells was through the CD58-CD2 affinity, and the binding interaction between the mannose and its receptor CD206 enhanced anchoring of manRTPNs to activated macrophages. Effective management was achieved through remodeling inflammation microenvironment. Basically, TPNs at RA sites shift core genes expression in three pathways including angiogenesis, bone resorption and cytokine secretion.

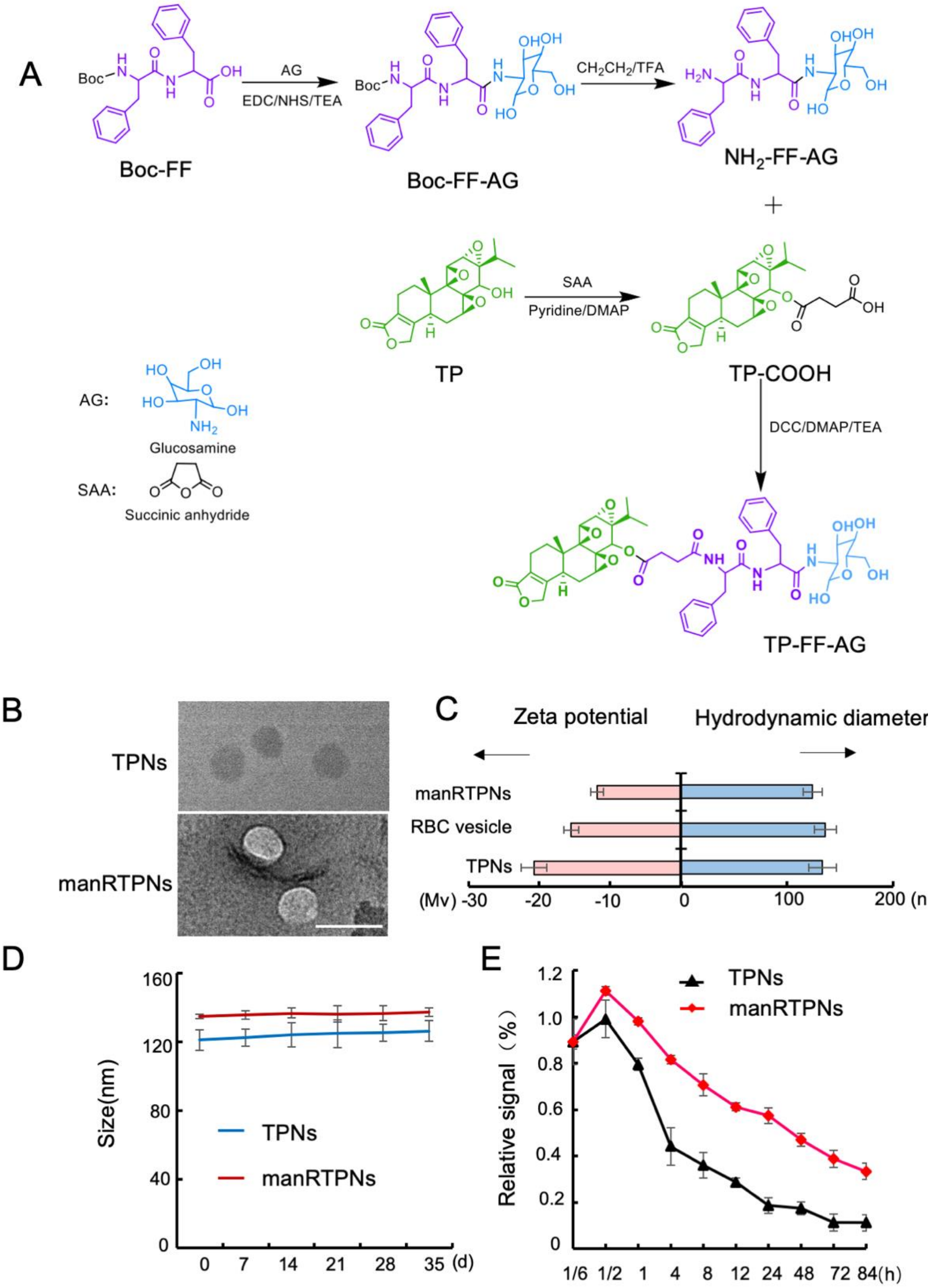

Figure 1. Preparation and Characterization of manRTPNs.

(A) Synthetic route illustration of triptolide self-assembling nanoparticles (TPNs). (B) Representative image of TPNs and manRTPNs examined with transmission electron microscopy (TEM). manRTPNs samples were stained with uranyl acetate. Scale bar, 200 nm.

(C) Size and ζ potential distribution of TPNs, RBC vesicles and manRTPNs. Each experiment had three replicates. (D) Stability of TPNs and manRTPNs in PBS over five weeks. Each experiment had three replicates. (E) Pharmacokinetics of TPNs and manRTPNs in vivo. Each experiment point had three replicates.

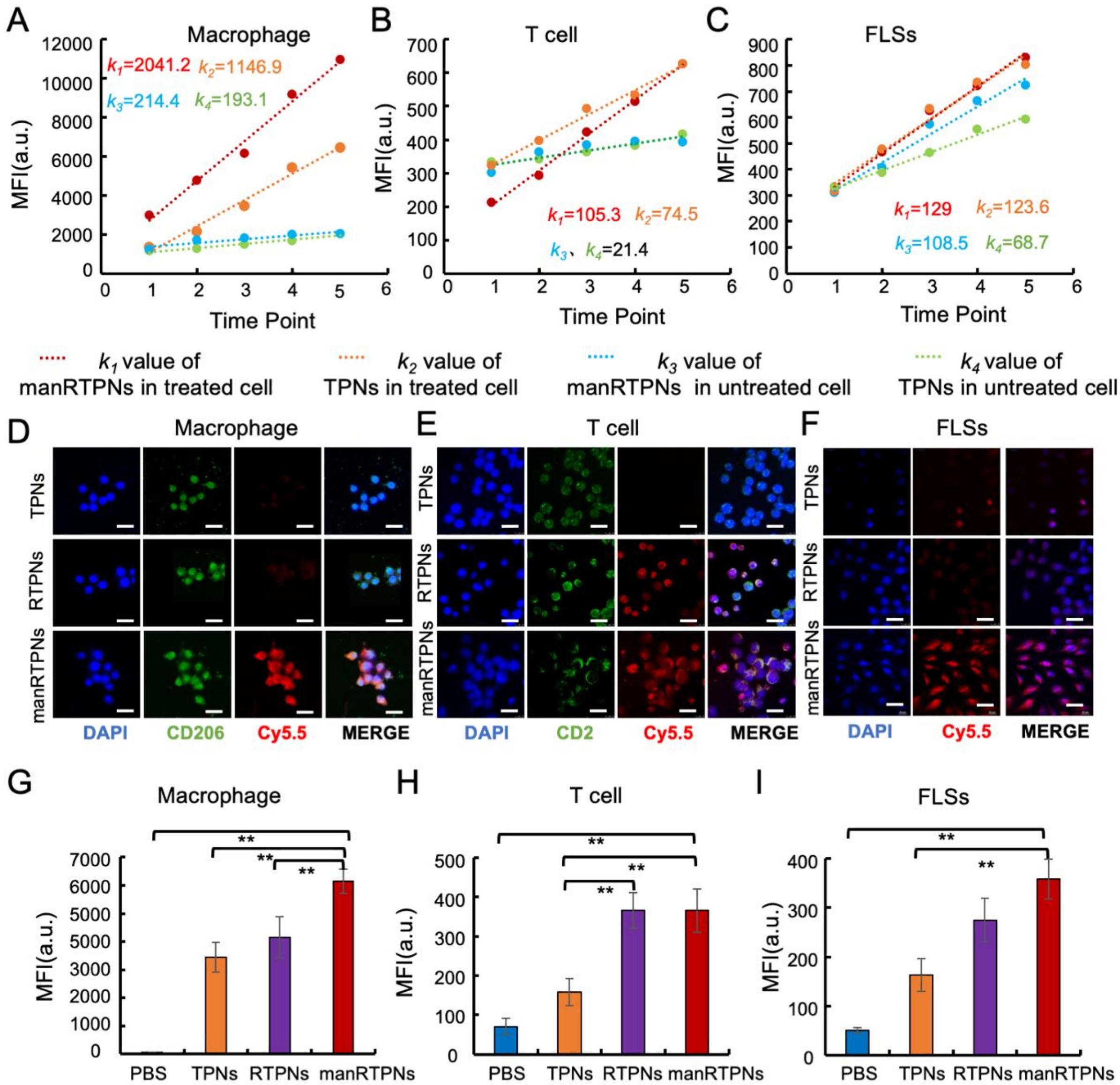

Figure 2. Targeting capacity to immune cells of manRTPNs.

(A-C) Cellular uptake capacity of TPNs and manRTPNs in three cell lines. Flow cytometry analysis of TPNs and manRTPNs were conducted in RAW246.7 (A), CTLL-2 (B) and RSC364 (C). k was slope of uptake curve built with mean fluorescence intensity (MFI) which indicated cell uptake rate. (D-F) Representative fluorescence images by confocal analysis. RAW246.7 (D), CTLL-2 (E), and RSC364 (F) were co-incubated with TPNs, RTPNs, and manRTPNs, respectively. Nanoparticles were labeled with Cy5.5 (red), CD206/CD2 antibody (green) expressed on the IL-4 -treated RAW264.7 and TNF-α treated CTLL-2 and cellular nuclear was labeled with DAPI (blue). Scale bars, 100 μm. (G-I) Flow cytometry analysis of RAW246.7 (G), CTLL-2 (H) and RSC364 (I) incubated with various nanoparticles. ** indicated significant difference and $p < 0.05$.

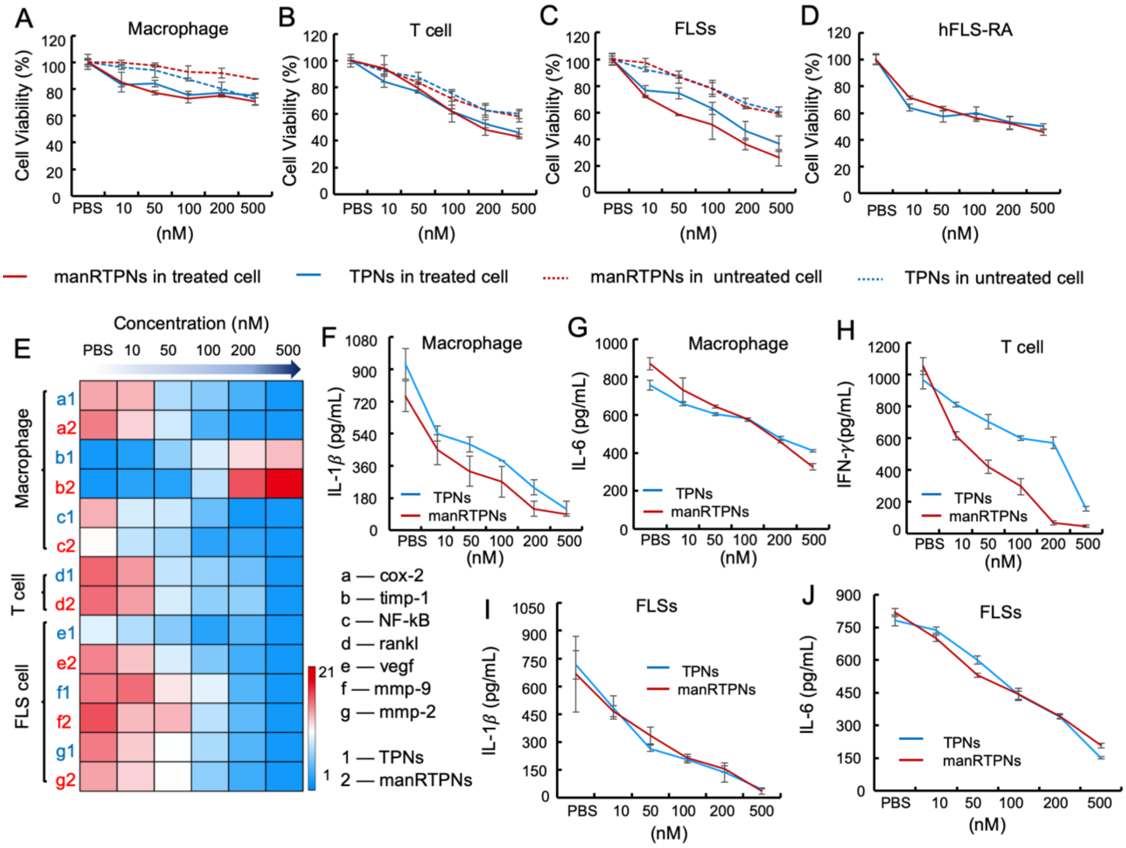

Figure 3. Efficacy of manRTPNs in inflammatory cells.

(A-D) Cytotoxicity of TPNs and manRTPNs in RAW264.7 (A), CTLL-2 (B), RSC364 (C), and hFLS-RA (D). Each experiment point had three replicates. (E) Heatmap of inflammatory factors genes expression. Briefly, genes cox-2, timp-1 and NF-κB were checked in RAW264.7, gene rankl was checked in CTLL-2 and genes vegf, mmp-9 and mmp-2 were checked in RSC364, respectively. (F-J) Cytokines concentration variation of inflammatory cells treated with TPNs and manRTPNs. Supernatant IL-1β was measured in RWA264.7 (F) and RSC364 (I), supernatant IL-6 in RWA264.7 (G) and RSC364 (J), supernatant IFN-γ in CTLL-2 (H), each experiment had three replicates.

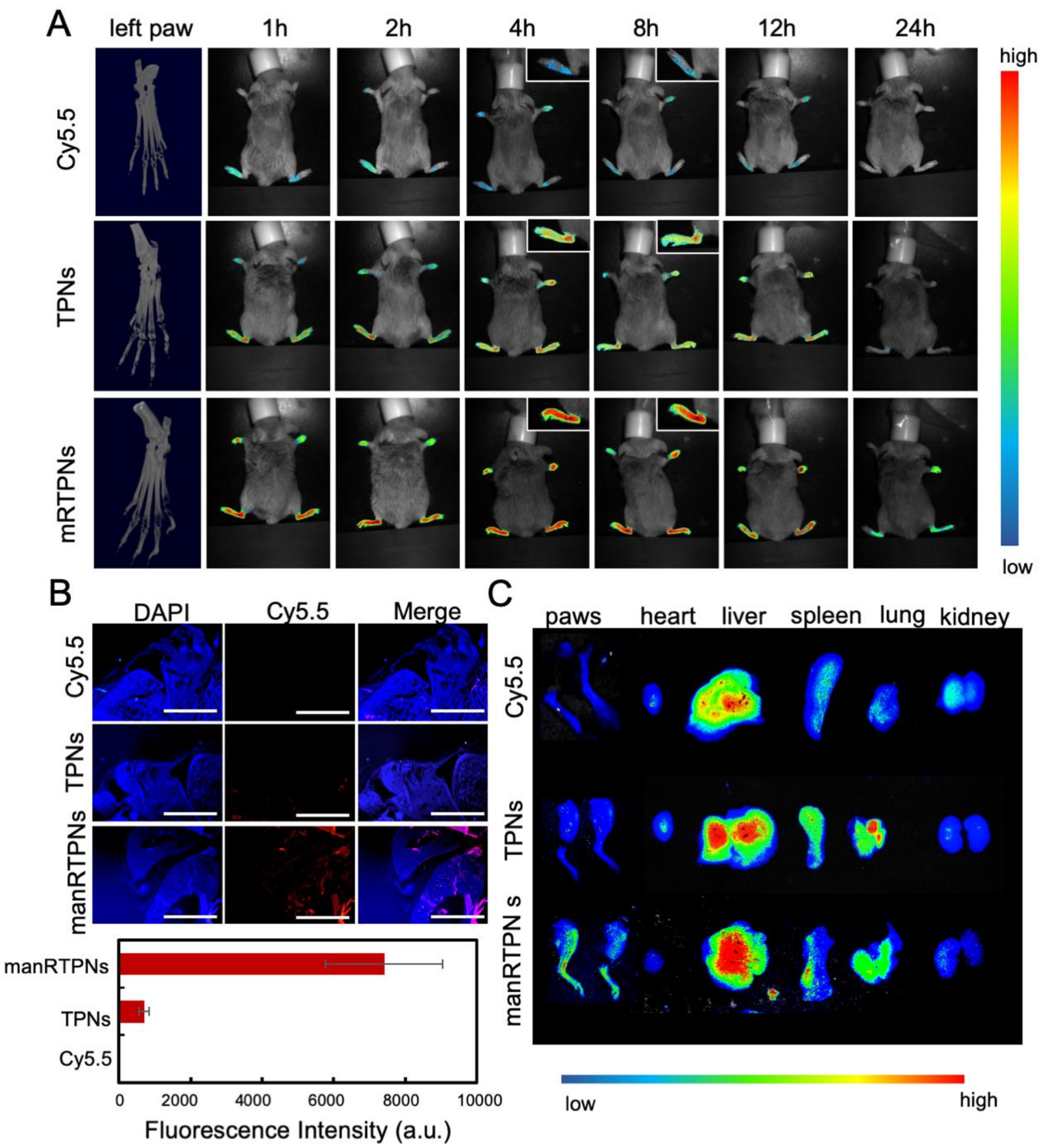

Figure 4. Targeting effect and accumulation at inflamed site of RA of manRTPNs.

(A) Representative images of free Cy5.5, TPNs and manRTPNs accumulating in arthritic paws. (B) Fluorescence images of free Cy5.5, TPNs and manRTPNs in arthritic paws fixed after 24 hours of intravenous injection. Scale bars, 500 μm. Fluorescence of free Cy5.5, TPNs and manRTPNs was quantified in arthritic paws sections. (C) Distribution of free Cy5.5, TPNs and manRTPNs in main organs and arthritic paws.

1

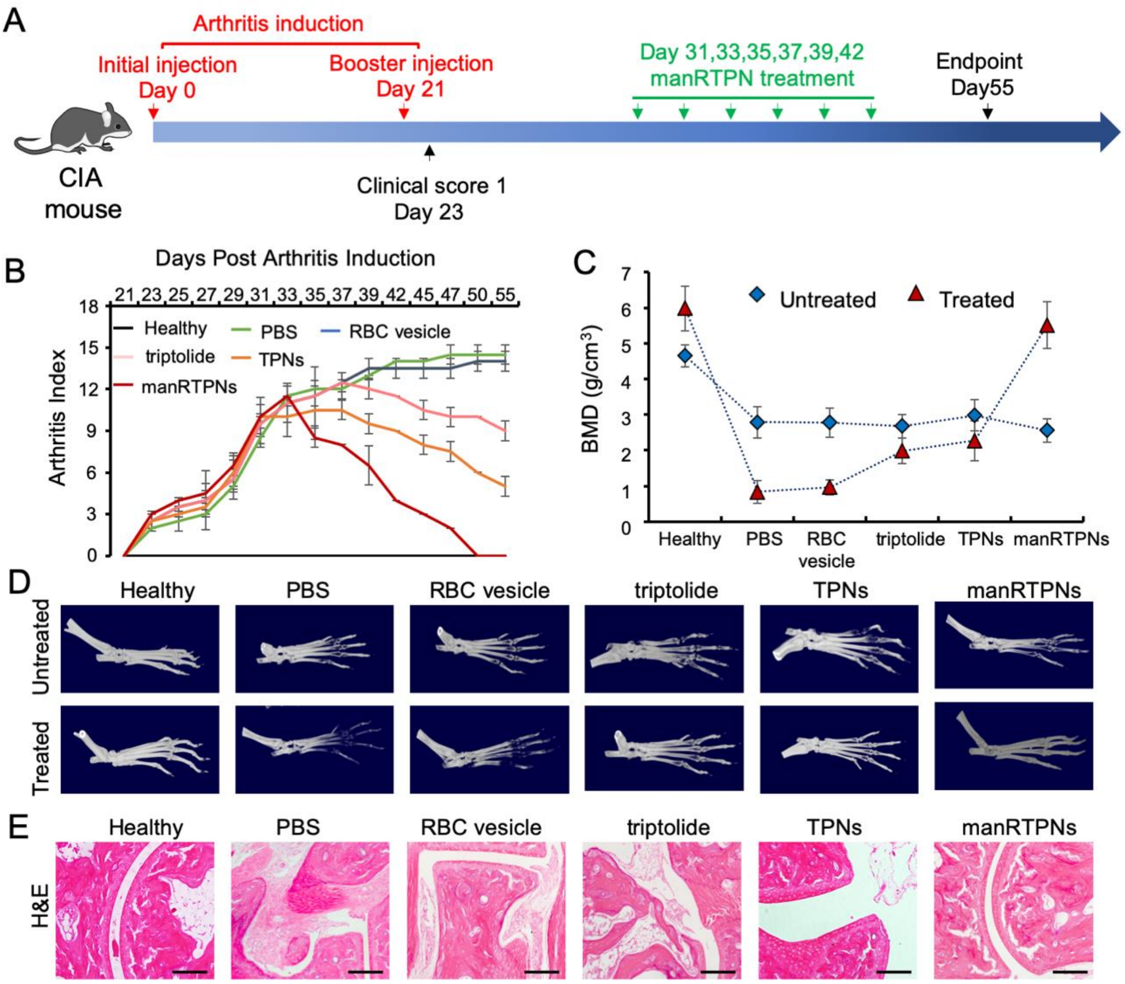

Figure 5. Therapeutic effect of manRTPNs in a mouse model of collagen-induced arthritis. (A) The study protocol of a therapeutic regimen with CIA mice model. (B) Arthritis indexes of different treatment groups over 14 days; each experiment had five mice replicates. (c) Bone mean density (BMD) variation of the mice paw joints before and after different treatment. (D) Representative 3D reconstructed bone images of arthritic paws in different treatment groups. (E) Representative images of H&E staining on knee sections from healthy mice and CIA mice treated with PBS, RBC vesicle, triptolide, TPNs or manRTPNs. Scale bars, 100 µm.

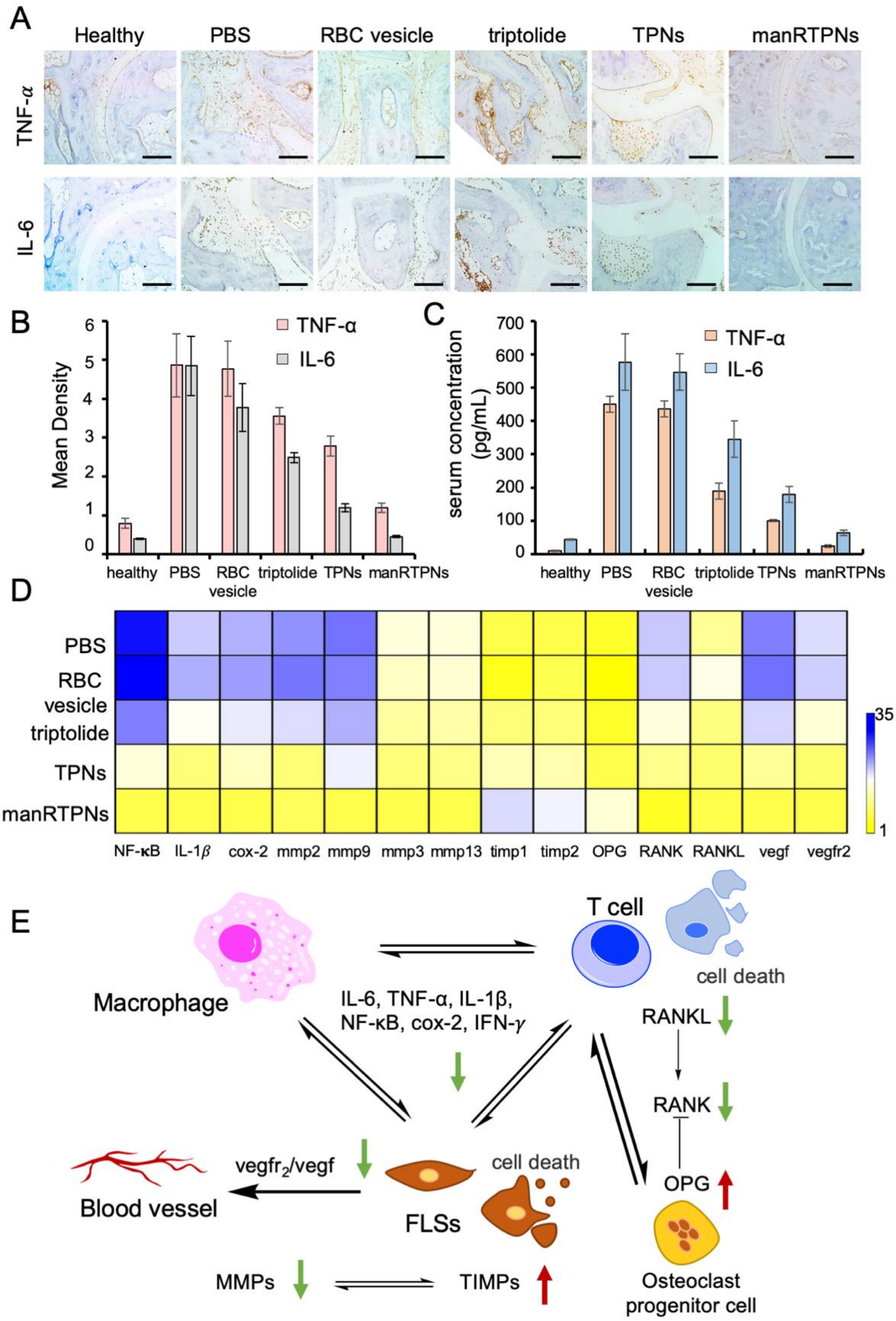

Figure 6. Remodeling inflammatory factor of RA treatment by manRTPNs.

(a) Representative images of TNF-α and IL-6 immunohistochemical staining on knee sections. Scale bars, 100 μm. (B) Immunohistochemical quantification of TNF-α and IL-6. (C) Serum concentration of TNF-α and IL-6 in healthy mice and CIA mice treated with different groups.

Each experiment point had three replicates. (D) Heatmap of genes expression profiles in different treatment.

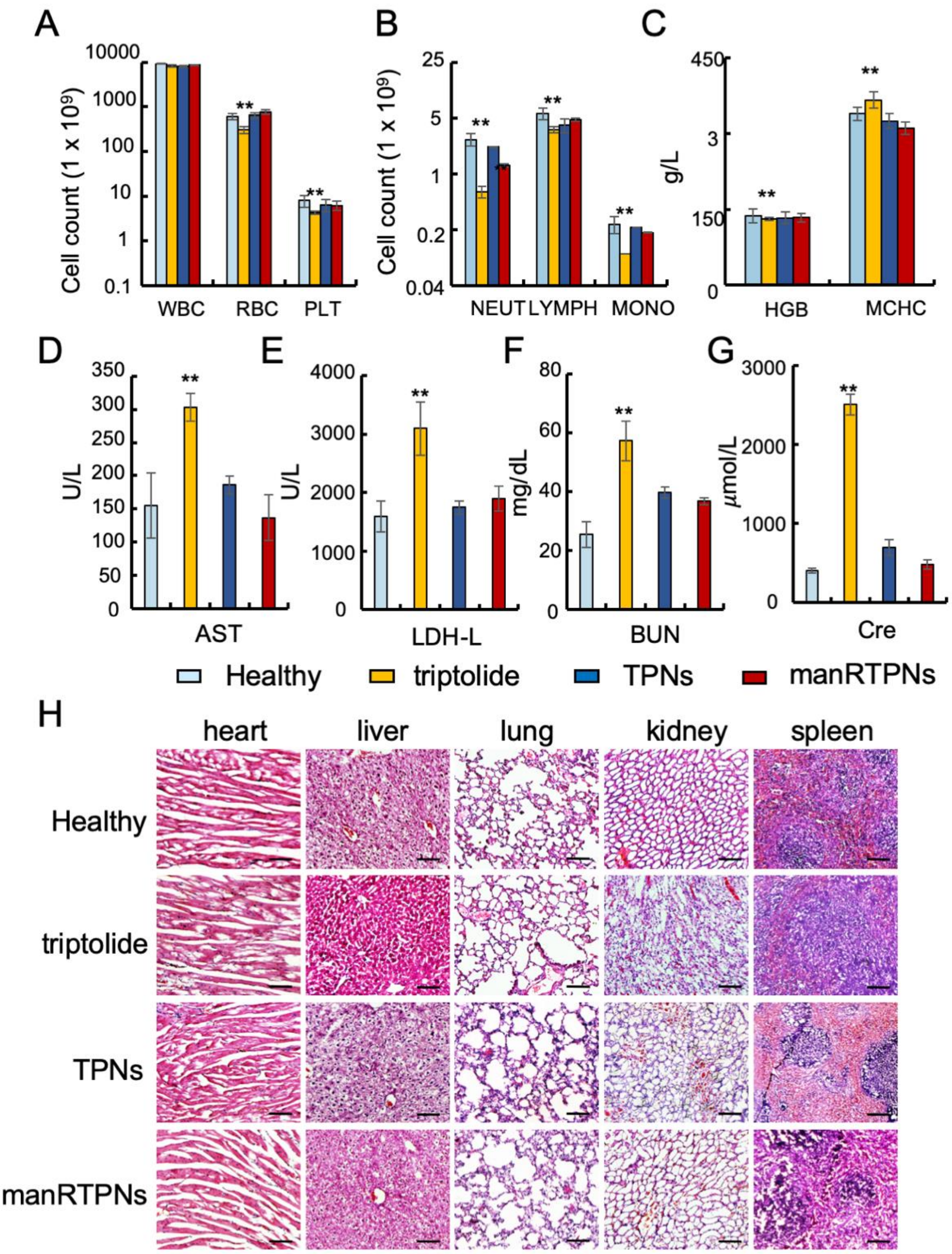

Figure 7. Biocompatibility and safety of manRTPNs.

(A) Complete cell counts (white blood cells, red blood cells, and platelets) in PBS and triptolide-, TPNs-, manRTPNs-treated groups. Experiment replicate, three. (B) Complete cell counts (neutrophil, lymphocyte, and monocyte) in PBS and triptolide-, TPNs-, manRTPNs-treated groups. Experiment replicate, three. (C) Concentration of HGB and MCHC in four groups indicated before. Experiment replicate, three. (D-G) Blood routine examination parameters including AST(D), LDH-L(E), BUN(F) and Cre(G) after different treatment. Experiment replicate, three. (H) H&E staining of main organs in four different groups. Scale bars, 100 μm.

1. Scott DL, Wolfe F, Huizinga TWJ. Rheumatoid arthritis. Lancet. 2010; 376: 1094-1108.
2. Van Vollenhoven RF. Treatment of rheumatoid arthritis: state of the art 2009. Nat Rev Rheumatol. 2009; 5: 531-541.
3. Bykerk V. Unmet needs in rheumatoid arthritis. J Rheumatol. 2009; 36: 42-46.
4. Salliot C, Van Der Heijde D. Long-term safety of methotrexate monotherapy in patients with rheumatoid arthritis: a systematic literature research. Ann Rheum Dis. 2009; 68: 1100-1104.
5. Alcorn N, Saunders S, Madhok R. Benefit-risk assessment of leflunomide an appraisal of leflunomide in rheumatoid arthritis 10 years after licensing. Drug Safety. 2009; 32: 1123-1134.
6. Leombruno JP, Einarson TR, Keystone EC. The safety of anti-tumour necrosis factor treatments in rheumatoid arthritis: meta and exposure-adjusted pooled analyses of serious adverse events. Ann Rheum Dis. 2009; 68: 1136-1145.
7. Hyrich KL, Watson KD, Isenberg DA, Symmons DPM, Register BB. The british society for rheumatology biologics register: 6 years on. Rheumatology. 2008; 47: 1441-1443.
8. Kirwan JR, Bijlsma JWJ, Boers M, Shea BJ. Effects of glucocorticoids on radiological progression in rheumatoid arthritis. Cochrane Db Syst Rev. 2007.
9. Ravindran V, Rachapalli S, Choy EH. Safety of medium- to long-term glucocorticoid therapy in rheumatoid arthritis: a meta-analysis. Rheumatology. 2009; 48: 807-811.

10. Zhang QZ, Dehaini D, Zhang Y, Zhou JL, Chen XY, Zhang LF, et al. Neutrophil membrane-coated nanoparticles inhibit synovial inflammation and alleviate joint damage in inflammatory arthritis. Nat Nanotechnol. 2018; 13: 1182-1190.
11. Li RX, He YW, Zhu Y, Jiang LX, Zhang SY, Qin J, et al. Route to rheumatoid arthritis by macrophage-derived microvesicle-coated nanoparticles. Nano Letters. 2019; 19: 124-134.
12. Liang HY, Peng B, Dong C, Liu LX, Mao JJ, Wei S, et al. Cationic nanoparticle as an inhibitor of cell-free DNA-induced inflammation. Nat Commun. 2018; 9: 4291.
13. Tao X, Cush J, Garret M, Pe. L. A phase I study of ethylacetate extract of the Chinese antirheumatic herb *Tripterygium wilfordii Hook F* in rheumatoid arthritis. J Rheumatol. 2001; 28: 2167.
14. Fan DP, Guo QQ, Shen JW, Zheng K, Lu C, Zhang G, et al. The effect of triptolide in rheumatoid arthritis: from basic research towards clinical translation. Int J Mol Sci. 2018; 19.
15. Pao HP, Liao WI, Wu SY, Hung KY, Huang KL, Chu SJ. PG490-88, a derivative of triptolide, suppresses ischemia/reperfusion-induced lung damage by maintaining tight junction barriers and targeting multiple signaling pathways. Int Immunopharmacol. 2019; 68: 17-29.
16. Chen YK, Zhang L, Ni JS, Wang XY, Cheng J, Li YC, et al. LLDT-8 protects against cerebral ischemia/reperfusion injury by suppressing post-stroke inflammation. J Pharmacol Sci. 2016; 131: 131-137.

17. He QL, Minn I, Wang QL, Xu P, Head SA, Datan E, et al. Targeted delivery and sustained antitumor activity of triptolide through glucose conjugation. Angew Chem Int Edit. 2016; 55: 12035-12039.
18. Yuan ZX, Wu XJ, Mo JX, Wang YL, Xu CQ, Lim LY. Renal targeted delivery of triptolide by conjugation to the fragment peptide of human serum albumin. Eur J Pharm Biopharm. 2015; 94: 363-371.
19. Mei ZN, Chen HB, Weng T, Yang YJ, Yang XL. Solid lipid nanoparticle and microemulsion for topical delivery of triptolide. Eur J Pharm Biopharm. 2003; 56: 189-196.
20. Huang CL, Zeng T, Li JW, Tan LS, Deng XL, Pan YC, et al. Folate receptor-mediated renal-targeting nanoplatform for the specific delivery of triptolide to treat renal ischemia/reperfusion injury. ACS Biomater Sci Eng. 2019; 5: 2877-2886.
21. Ling D, Xia H, Park W, Hackett MJ, Song C, Na K, et al. pH-sensitive nanoformulated triptolide as a targeted therapeutic strategy for hepatocellular carcinoma. ACS Nano. 2014; 8: 8027-8039.
22. Xu HT, Liu B. Triptolide-targeted delivery methods. Eur J Med Chem. 2019; 164: 342-351.
23. Abbas M, Zou QL, Li SK, Yan XH. Self-assembled peptide- and protein-based nanomaterials for antitumor photodynamic and photothermal therapy. Adv Mater. 2017; 29.

24. Zhu PL, Yan XH, Su Y, Yang Y, Li JB. Solvent-induced structural transition of self-assembled dipeptide: from organogels to microcrystals. Chem-Eur J. 2010; 16: 3176-3183.

25. Yan XH, Zhu PL, Li JB. Self-assembly and application of diphenylalanine-based nanostructures. Chem Soc Rev. 2010; 39: 1877-1890.

26. Elshabrawy HA, Chen ZL, Volin MV, Ravella S, Virupannavar S, Shahrara S. The pathogenic role of angiogenesis in rheumatoid arthritis. Angiogenesis. 2015; 18: 433-448.

27. Kinne RW, Brauer R, Stuhlmuller B, Palombo-Kinne E, Burmester GR. Macrophages in rheumatoid arthritis. Arthritis Res. 2000; 2: 189-202.

28. Davis SJ, Ikemizu S, Evans EJ, Fugger L, Bakker TR, Van Der Merwe PA. The nature of molecular recognition by T cells. Nat Immunol. 2003; 4: 217-224.

29. Raychaudhuri S, Thomson BP, Remmers EF, Eyre S, Hinks A, Guiducci C, et al. Genetic variants at CD28, PRDM1 and CD2/CD58 are associated with rheumatoid arthritis risk. Nat Genet. 2009; 41: 1313-1318.

30. Sable R, Durek T, Taneja V, Craik DJ, Pallerla S, Gauthier T, et al. Constrained cyclic peptides as immunomodulatory inhibitors of the CD2:CD58 protein-protein interaction. ACS Chemical Biology. 2016; 11: 2366-2374.

31. Hu CMJ, Fang RH, Copp J, Luk BT, Zhang LF. A biomimetic nanosponge that absorbs pore-forming toxins. Nat Nanotechnol. 2013; 8: 336-340.

32. Rossi L, Fraternale A, Bianchi M, Magnani M. Red blood cell membrane processing for biomedical applications. Front Physiol. 2019; 10.

33. He QL, Titov DV, Li J, Tan MJ, Ye ZH, Zhao YM, et al. Covalent modification of a cysteine residue in the XPB subunit of the general transcription factor TFIIH through single epoxide cleavage of the transcription inhibitor triptolide. Angew Chem Int Edit. 2015; 54: 1859-1863.
34. Hu CMJ, Zhang L, Aryal S, Cheung C, Fang RH, Zhang LF. Erythrocyte membrane-camouflaged polymeric nanoparticles as a biomimetic delivery platform. P Natl Acad Sci USA. 2011; 108: 10980-10985.
35. Fang RNH, Hu CMJ, Chen KNH, Luk BT, Carpenter CW, Gao WW, et al. Lipid-insertion enables targeting functionalization of erythrocyte membrane-cloaked nanoparticles. Nanoscale. 2013; 5: 8884-8888.
36. Shao F, Wang GJ, Xie HT, Zhu XY, Sun JG, A JY. Pharmacokinetic study of triptolide, a constituent of immunosuppressive chinese herb medicine, in rats. Biol Pharm Bull. 2007; 30: 702-707.
37. Ghosh S, Hayden MS. New regulators of NF-kappaB in inflammation. Nat Rev Immunol. 2008; 8: 837-848.
38. Niedermeier M PT, Korb A. Therapeutic opportunities in fibroblasts in inflammatory arthritis. Best Pract Res Clin Rheumatol. 2010; 24: 527-540.
39. Brand DD, Latham KA, Rosloniec EF. Collagen-induced arthritis. Nat Protoc. 2007; 2: 1269-1275.
40. Noack M, Miossec P. Selected cytokine pathways in rheumatoid arthritis. Seminars in Immunopathology. 2017; 39: 365-383.

41. Geusens P. The role of RANK ligand/osteoprotegerin in rheumatoid arthritis. Ther Adv Musculoskelet Dis. 2012; 4: 225-233.

42. Chen L, Deng H, Cui H, Fang J, Zuo Z, Deng J, et al. Inflammatory responses and inflammation-associated diseases in organs. Oncotarget. 2018; 9: 7204-7218.